Materials Advances

ROYAL SOCIETY OF CHEMISTRY

PAPER

View Article Online
View Journal | View Issue

Cite this: *Mater. Adv.*, 2025, 6, 2056

Highly elastic polyvinyl alcohol embolic microspheres for effective transarterial embolization†

Li Liu,‡[ae] Xiangxian Xu,‡[d] Xiaoli Zhu,‡[e] Meng Dang,[b] Yunming Zhang,[a] Donghong Shi,[a] Shenzhe Liu,[b] Zhiwei Zhang,[b] Jing Pan,[a] Jing Zhong,[a] Lin Ou-yang,*[c] Zhaogang Teng *[b] and Longjiang Zhang *[a]

Transarterial embolization therapy is a highly promising, minimally invasive interventional procedure for treating vascular and neoplastic diseases in the clinic. The use of highly elastic and deformable embolization microspheres is crucial for ensuring smooth delivery through a catheter and achieving complete endovascular embolization. In this study, a polyvinyl alcohol embolic microsphere, MegaSphere, with exceptional elasticity was used for vascular embolization. The results obtained from an *in vitro* embolization model demonstrated the good stability and elastic deformation ability of MegaSphere. These properties allow these spheres to aggregate tightly and effectively embolize blood vessels at different levels. Furthermore, in a rabbit model, we achieved highly efficient renal embolization *via* MegaSphere. These microspheres could reach the distal vessels of the renal artery and effectively embolize small arteries within the renal cortex, resulting in complete terminal embolization. Substantial necrosis of the renal parenchyma was observed within seven days after embolization, indicating an excellent embolization effect. Moreover, in a rabbit model with liver VX2 transplant tumors, the use of drug-loaded MegaSphere-doxorubicin microspheres demonstrated strong efficacy in antitumor chemoembolization therapy. Through blockade of the tumor blood supply and increased local chemotherapy, effective inhibition of liver tumor progression was achieved within seven days following transcatheter arterial chemoembolization (TACE). In conclusion, this study highlights the promising potential of MegaSphere as an embolic agent with potential for clinical translational applications.

Received 22nd January 2025,
Accepted 12th February 2025

DOI: 10.1039/d5ma00057b

rsc.li/materials-advances

1. Introduction

Transarterial embolization therapy is a minimally invasive interventional procedure that involves the delivery of embolic materials to block blood vessels.[1,2] This method is widely utilized in the treatment of tumors, various hemorrhagic diseases, and vascular abnormalities, particularly in the context of transarterial chemoembolization (TACE) for neoplastic diseases.[3–6] By obstructing the artery that supplies the tumor, embolic agents effectively block both the nutrient supply and blood supply to the tumor.[7] This process results in tumor necrosis and subsequent shrinkage.[8] Simultaneously, these embolic agents facilitate the delivery of drugs to local tumor tissue, thereby achieving a synergistic antitumor effect through a combination of embolization and targeted chemotherapy.[9] However, owing to the heterogeneity in the size and internal structure of target lesion vessels, most embolic materials still require optimization for effective application in TACE.[10] This need is particularly evident in areas such as distal delivery, terminal embolization, and excellent drug loading and release capabilities.[10] Embolic microspheres are a novel class of vascular embolic agents with distinct advantages over traditional agents such as lipiodol emulsions.[11] These microspheres exhibit superior vascular targeting and drug delivery capabilities, making them highly suitable for use in TACE procedures.[12] Nonetheless, further optimization of the performance of embolic microspheres to increase the distal embolization efficacy and promote the local drug treatment effects is necessary. This optimization will

[a] *Department of Radiology, Jinling Hospital, Affiliated Hospital of Medical School, Nanjing University, Nanjing 210002, P. R. China. E-mail: kevinzhlj@163.com*
[b] *Key Laboratory for Organic Electronics and Information Displays and Jiangsu Key Laboratory for Biosensors, Institute of Advanced Materials, Jiangsu National Synergetic Innovation Centre for Advanced Materials, Nanjing University of Posts and Telecommunications, Nanjing 210023, P. R. China. E-mail: iamzgteng@njupt.edu.cn*
[c] *Department of Radiology, The 909th Hospital, School of Medicine, Xiamen University, Zhangzhou 363020, P. R. China. E-mail: ddcqzg@126.com*
[d] *Department of Radiology, Jiangsu Province Hospital of Chinese Medicine, Affiliated Hospital of Nanjing University of Chinese Medicine, Nanjing 210029, P. R. China*
[e] *Department of Interventional Radiology, The First Affiliated Hospital of Soochow University, Suzhou 215006, P. R. China*

† Electronic supplementary information (ESI) available. See DOI: https://doi.org/10.1039/d5ma00057b

‡ These authors contributed equally to this work.

contribute to the goal of achieving highly effective intra-arterial embolization therapy.[13]

The efficacy of arterial embolization therapy strongly depends on the performance of the embolic microspheres.[14–16] Previous studies have investigated various types of embolic microspheres with different performances, including agents with different materials, size ranges, variations in drug loading and release capabilities, degrees of degradability, magnetic imaging capabilities, and, more recently, X-ray imaging capabilities.[17–26] However, in the context of applications involving the delivery of microspheres through catheter arteries for vessel occlusion, other less studied characteristics of microspheres, such as their mechanical stability and elastic deformation ability, have become important.[27] It is speculated that highly elastic microspheres can effectively fill vascular lumens at different levels, thereby achieving the objective of completely obstructing the blood supply to the target vessel. Additionally, embolic microspheres with excellent drug loading and release properties can substantially increase the effectiveness of antitumor chemotherapy embolization. In recent years, there has been increased interest in multifunctional embolic microspheres for intra-arterial embolization therapy.[28,29] However, to our knowledge, the application of highly elastic microspheres specifically for achieving effective embolization in arterial embolization therapy has not been reported.

Here, we investigate a new type of embolic microsphere called MegaSphere, which has excellent mechanical stability and elastic deformation ability. For the first time, we observed in an *in vitro* embolization model that MegaSphere transforms from a spherical shape to an elliptical or even flat shape under external forces, achieving seamless filling inside capillary glass tubes. Moreover, MegaSphere achieved complete occlusion of the portal vein lumen in a decellularized liver model. Furthermore, MegaSphere strongly increases the drug loading capacity of the microspheres and provides a foundation for combination therapy with drugs. We further conducted *in vivo* embolization experiments in rabbits to further validate the exceptional elastic deformation ability of MegaSphere. The results demonstrated its capacity to adapt to vessels at various levels and effectively reach the lumens of the distal branching vessels of the renal artery. Consequently, complete necrosis of the embolized tissue was achieved, highlighting the efficacy of MegaSphere in arterial embolization therapy. Additionally, in a study using a rabbit liver VX2 tumor transplantation model, drug-loaded MegaSphere microspheres showed highly effective antitumor therapeutic effects when used in TACE. In summary, the highly elastic MegaSphere microspheres not only enable embolization at different vascular levels but also facilitate drug-loaded chemotherapy embolization for antitumor treatment.

2. Materials and methods

2.1. Materials and animals

Doxorubicin hydrochloride (Dox) was purchased from Hisun Pharmaceutical Co., Ltd (Zhejiang, China). Maleimide derivative cyanine dye (Cy5.5-maleimide) was provided by Seebio Biotechnology Co., Ltd (Shanghai, China). Dulbecco's modified Eagle's medium (DMEM), phosphate-buffered saline (PBS), Cell Counting Kit-8 (CCK-8) assays, a live/dead cell double-staining kit, and a 4% paraformaldehyde fixation solution were purchased from Nanjing Keygen Biotech. Co., Ltd (Nanjing, China). Heat-inactivated fetal bovine serum (FBS) and penicillin–streptomycin solution were acquired from Gibco Laboratories (NY, USA). Deionized water with a resistivity of 18 Ω m (Millipore) was utilized for all the experiments. Isoflurane was obtained from Yuyan Scientific Instrument Co., Ltd (Shanghai, China). Polyoxyethylene ether (Triton X) and sodium dodecyl sulfate (SDS) were procured from Yun Crown Biotechnology Co., Ltd (Shanghai, China). Iopromide was purchased from Bayer Pharmaceutical Co., Ltd (Guangdong China). MegaSphere was obtained from Nanjing Xiaowei Co., Ltd (Jiangsu, China). CalliSphere (specification 100–300 μm) was obtained from Suzhou Hengrui Garishen Biomedical Technology Co., Ltd (Jiangsu, China). DC Bead (100–300 μm) was obtained from Biocompatibles UK, Ltd (Surrey, UK). The enzyme-linked immunosorbent assay (ELISA) kits for TNF-α, IL-1β, IL-6, and PCT in rabbits were purchased from Shanghai Enzyme-Linked Biotechnology Co., Ltd (Shanghai, China). The anti-Ki67 rabbit pAb, anti-CD31 rabbit pAb, anti-HIF-1α rabbit pAb, recombinant anti-vascular endothelial growth factor (anti-VEGF) antibody and terminal deoxynucleotidyl transferase-mediated deoxyuridine triphosphate nick end labeling (TUNEL) kit were obtained from Servicebio Technology Co., Ltd (Wuhan, China). All Sprague–Dawley rats (SD, 2–3 months old, weighing 200–250 g) were obtained from Jiangsu Huachuang XinNuo Biotechnology Co., Ltd (Nanjing, China). All New Zealand white rabbits, regardless of sex and weighing 2.5–3.0 kg, were procured from Nanjing Laboratory Animal Co. Ltd (Nanjing, China).

2.2. Characterization of MegaSphere

An optical microscope (IX71; Olympus, Tokyo, Japan) was used to observe the color, shape and size distribution of the MegaSphere microspheres. ImageJ software was used for statistical analysis of the particle size of the MegaSphere microspheres. A fluorescence microscope from Olympus (Tokyo, Japan) was used to observe the MegaSphere microspheres after loading with Dox. A confocal laser microscope (FV1000, Olympus Corporation, Germany) was used to capture cross-sectional fluorescence images of MegaSphere loaded with Dox or Cy5.5. The surface of MegaSphere was characterized *via* a scanning electron microscope (Hitachi S4800 microscope, Tokyo, Japan). Fourier transform infrared (FTIR) spectra were recorded *via* a NEXUS870 spectrometer (Nicolet Instruments, Inc., Madison, WI, USA) to analyze the chemical functional groups present within MegaSphere.

2.3. Evaluation of the elastic capacity of MegaSphere

The solution containing the MegaSphere microspheres was carefully dispensed on a glass dish placed on the microscope table *via* a micropipette. The field of view of the microscope was adjusted, and a microvascular clamp was employed to secure a MegaSphere particle in place. A specific amount of force was applied to compress the microsphere, inducing deformation, and the maximum degree of deformation was observed and recorded. The clamp was subsequently gradually released to

observe the process of the MegaSphere returning to its original shape, and its final state was observed and documented. This procedure was used to assess the elasticity and shape recovery ability of the MegaSphere microspheres. Young's modulus of the MegaSphere microspheres was evaluated using a nanoindentation test to quantitatively analyze their deformability. This study provides valuable insights into their deformability and ability to regain their original shape after deformation, contributing to the overall assessment of their elastic properties.

2.4. Embolization of MegaSphere in a capillary glass tube

Capillary glass tubes were used to simulate and test the embolization of small blood vessels by MegaSphere microspheres *in vitro*. A certain amount of Dox-loaded MegaSphere particles was suspended in PBS to prepare a concentration of 1 mg mL^{-1}. Then, a syringe was filled with the MegaSphere-Dox suspension, and the suspension was carefully injected into a capillary glass tube with a gradually narrowing diameter at a controlled injection rate of 1 mL min^{-1}. The liquid from the syringe flowed out through the narrower tip of the capillary glass tube, effectively filling the capillary lumen with MegaSphere-Dox particles. The filling effect of MegaSphere-Dox particles within the capillary glass tube and the deformation of MegaSphere-Dox inside the tube were determined *via* fluorescence microscopy.

2.5. Embolization experiments of MegaSphere microspheres in decellularized livers

All animal experimental procedures were reviewed and approved by the Animal Protection Committee of Jinling Hospital, which is affiliated with Nanjing University. The animal experiments were conducted in strict accordance with the guidelines provided by the Animal Protection Committee (Approval no. 2023JLHGZRDWLS-00048). Fresh and intact livers were obtained from SD rats through abdominal dissection following euthanasia. The obtained fresh liver tissues were thoroughly washed with PBS. The livers were subsequently perfused through the portal vein *via* the following solutions: distilled water (0.5 h), 4% polyoxyethylene ether (Triton X) aqueous solution (3 h), and 0.5% SDS aqueous solution (12 h), with a flow rate of 6 mL min^{-1}.[30,31] The perfusion process continued until the livers became transparent. A suspension of MegaSphere-Dox microspheres with a volume of 4 mL (concentration of 1 mg mL^{-1}) was injected into the decellularized liver through the main trunk of the portal vein at a controlled injection rate of 1 mL min^{-1}. Finally, the decellularized liver perfused with MegaSphere-Dox microspheres was examined and characterized *via* fluorescence microscopy. The filling and distribution of MegaSphere-Dox microspheres within the lumens of various branches of the portal vein were assessed, and this experimental procedure was repeated three times to ensure reliable results and consistency.

2.6. Dox loading and release

The drug loading efficacy of the MegaSphere microspheres was analyzed through a Dox loading test. Initially, Dox (10 mg) was completely dissolved in PBS (5 mL). Subsequently, 100 mg of MegaSphere microspheres was added to the Dox solution and thoroughly mixed to ensure loading of the drug. Similarly, Dox (10 mg) was added to PBS (5 mL) and completely dissolved. Then, 100 mg of CalliSphere microspheres was added to the Dox solution and thoroughly mixed. The supernatants were collected at specific time points (5, 10, 20, 30, and 60 min) after shaking and centrifugation. The absorbance of the Dox solutions at 482 nm was measured *via* a UV-visible spectrophotometer (PerkinElmer Lambda 35 spectroscope, USA). The drug loading efficiency was calculated *via* the following formula: drug loading efficiency (wt%) = [(mass of the added drug − mass of drug in the sample solution and washing solution)/mass of the added drug] × 100%. This loading experiment was repeated three times to ensure the consistency and reliability of the results.

For a comparative analysis of the drug release performance of MegaSphere-Dox and CalliSphere-Dox, 100 mg of each microsphere type (MegaSphere-Dox and CalliSphere-Dox) was immersed in 10 mL of FBS solution. The drug release test was conducted at 37 °C using a release medium consisting of FBS solution (5% saline, pH 7.4). The Dox-loaded microspheres were collected at the bottom of the tube *via* centrifugation at predetermined time intervals (1, 2, 3, 4, 5, 6, 7, and 8 days). At each time point, the supernatant was collected, and an equal amount of fresh FBS solution was added. The absorbance of Dox in the supernatant was measured at 482 nm *via* a UV-visible spectrophotometer. All release experiments were repeated three times to ensure the accuracy and reliability of the results.

2.7. *In vitro* hemolysis experiment

An *in vitro* hemolysis test was conducted to evaluate the hemolytic properties of MegaSphere. Fresh blood was collected from the marginal ear vein of healthy rabbits and transferred to blood collection tubes containing heparin sodium as an anticoagulant. The noncoagulated blood was subjected to centrifugation at 3000 rpm for 15 min to separate the supernatant. The resulting red blood cells were then resuspended in PBS. This resuspension process was repeated three times until the supernatant became clear. Finally, the red blood cells were resuspended in PBS to create a 2% red blood cell suspension, which was used for subsequent hemolysis testing. MegaSphere microspheres were prepared as 1 mL PBS suspensions with various concentrations, including 0, 1, 2, 4, 8, 10, and 15 mg mL^{-1}. Next, 500 μL of the prepared 2% red blood cell suspension was added to each group of MegaSphere suspensions. After the suspensions were incubated in a 37 °C incubator for 2 h, the supernatant was collected *via* centrifugation at 3000 rpm for 15 min. The absorbance value of the collected supernatant was measured *via* a microplate reader at a wavelength of 540 nm. A 2% red blood cell suspension in PBS was used as the negative control group, whereas a 2% red blood cell suspension in deionized water served as the positive control group. Each experiment was repeated three times. The hemolysis ratio was calculated *via* the following formula:

$$\text{Hemolysis ratio (\%)} = (OD_{sample} - OD_{negative})/(OD_{positive} - OD_{negative}) \times 100$$

where OD_{sample}, $OD_{negative}$, and $OD_{positive}$ represent the absorbance values of the sample group, negative control group, and positive control group, respectively.

2.8. Cell culture

Human liver cancer HepG2 cells were procured from the American Type Culture Collection (ATCC, Manassas, VA). The cells were cultured in DMEM supplemented with 10% FBS and 1% penicillin/streptomycin. The cell culture was maintained at 37 °C in a 5% carbon dioxide (CO_2) environment.

2.9. Cytotoxicity of MegaSphere

The cytotoxicity of MegaSphere was evaluated through an *in vitro* test with HepG2 cells. In brief, HepG2 cells were seeded in 96-well plates at a density of 1×10^4 cells per well and incubated for 24 h in a humidified atmosphere with 5% CO_2. The MegaSphere microspheres were subsequently sterilized and prepared as a mixed solution with fresh medium. The medium in the 96-well plates was replaced with 200 μL of fresh medium containing different concentrations of MegaSphere (0, 1, 2, 4, 8, 10, and 15 mg mL^{-1}). The cells were allowed to incubate for an additional 24 and 48 h. Finally, *in vitro* cytotoxicity was evaluated *via* the CCK-8 assay. The experimental setup included a blank control group consisting of pure medium (without cells), a negative control group where the cells were treated with pure medium, and a positive control group where the cells were treated with fresh medium containing MegaSphere. Then, 10 μL of CCK-8 reagent was added to each well, and the cells were incubated for another 4 h. The absorbance of each well was measured *via* a microplate reader at a wavelength of 570 nm (BioTek Instruments, Winooski, VT, USA). Three different replicate wells were used for each concentration. Cell viability, expressed as a percentage of the control, was calculated according to the following formula:

$$\text{Cell viability}\,(\%) = (\text{OD}_{\text{sample}} - \text{OD}_{\text{blank}})/(\text{OD}_{\text{negative}} - \text{OD}_{\text{blank}}) \times 100\%$$

In the equation, $\text{OD}_{\text{sample}}$ represents the positive control group, $\text{OD}_{\text{negative}}$ represents the negative control group, and OD_{blank} represents the blank control group.

Additionally, the HepG2 cells were stained with calcein AM and propidium iodide (PI) to perform a live/dead cell assay and analyze cell viability. HepG2 cells were seeded in 24-well plates at a density of 5×10^4 cells per well and incubated for 24 h in a humidified atmosphere with 5% CO_2. The medium was subsequently removed, and the cells were washed with PBS. MegaSphere microspheres were prepared in solutions of various concentrations (0, 8, 10, and 15 mg mL^{-1}) in fresh medium. One milliliter of solution containing different concentrations of MegaSphere was added to each well of a 24-well plate. The cells were then incubated in a cell culture incubator for an additional 24 h. After incubation, the medium was removed, and the cells were washed with PBS to remove the MegaSphere from the wells. Based on the instructions provided with the reagent, the calcein AM/PI working solution was prepared. Subsequently, 250 μL of the prepared solution was added to each well of the 24-well plate. The cells were incubated at 37 °C for 10–20 min. After the incubation period, any excess staining solution was washed off with PBS. The cell staining results and cell viability were then determined with a fluorescence microscope.

2.10. Evaluation of the *in vitro* antitumor effects

The *in vitro* antitumor effects of MegaSphere-Dox were evaluated in HepG2 cells. The cells were seeded in 96-well plates at a density of 1×10^4 cells per well, and 200 μL of medium was added to each well. The cells were cultured and incubated at 37 °C with 5% CO_2 for 24 h. Subsequently, the original medium was removed, and the cells were washed three times with PBS. Two hundred microliters of fresh medium containing different concentrations of MegaSphere-Dox were subsequently added to each well. The concentration gradient of MegaSphere-Dox used in the experiment was as follows: 0, 0.0125, 0.025, 0.05, 0.1, and 0.2 mg mL^{-1}. After coincubation for 24 h, the medium and MegaSphere microspheres in each well were carefully removed, and the cells were subsequently washed three times with PBS to remove any residual substances. The viability of the HepG2 cells was then measured *via* a CCK-8 assay. The experiment was repeated three times to ensure the accuracy and reproducibility of the results.

2.11. Renal artery embolization *in vivo*

Twelve healthy New Zealand white rabbits, with a weight of 2.5 to 3.0 kg, were chosen for the experiment. The rabbits were selected regardless of sex and were divided into three test groups: the MegaSphere group, the CalliSphere group and the DC Bead group. Additionally, a blank control group, in which normal saline was injected through the renal artery, was included in the experiment. Each group consisted of three rabbits. Digital subtraction angiography (DSA) was utilized to guide the interventional procedures for all experimental animals. The rabbits were subjected to a 12 h fast period prior to the procedure and were then anesthetized with 5% isoflurane for induction and 3.5% isoflurane for maintenance. The rabbits were placed in a supine position on the work table, and blood samples were collected from the marginal ear vein prior to surgery. These blood samples were used for routine blood tests, coagulation tests, blood biochemical analysis, and relevant inflammatory factor assays. During the interventional procedure, the right femoral artery was initially exposed. A 4F catheter sheath was subsequently inserted into the femoral artery, guided by a guide wire. The guide wire and 4F catheter were advanced to the abdominal aorta. A total of 4 mL of iopromide was subsequently injected for celiac artery angiography at a rate of 1.0 mL s^{-1} *via* a high-pressure injector. This procedure allowed visualization of the distribution of the celiac artery and facilitated the identification of the opening of the renal artery. A 2.6-F microcatheter system was subsequently advanced into the renal artery in a slow and controlled manner. This system allowed superselective renal artery angiography, ensuring careful confirmation of the renal artery branches and the precise positioning of the microcatheter. Finally, 2 mL of the microsphere suspension from each experimental group was injected into one renal artery *via* a renal arterial catheter. This process ensured delivery of the microspheres to the targeted renal artery in each group. The solvent used for each microsphere suspension was a mixture of iopromide and PBS, with a concentration of 10 mg mL^{-1}. The injection of the microspheres into the

renal artery was performed over a period of 2 min. After the injection of the microspheres, arterial catheter angiography was performed once again on the rabbits' abdominal aorta. This procedure was performed to observe the renal blood supply following the embolization procedure. On the seventh day after the embolization procedure, a full-body CT scan was conducted on the rabbits in each group. This CT scan was used to provide a CT image of each organ and evaluate the presence of any off-target embolization. Blood samples were collected from the rabbits 7 days post-operation for routine blood tests, coagulation tests, blood biochemical analysis, and relevant inflammatory factor assessments. A comparison was made between the presurgery and postsurgery indicators to assess the impact of embolization on organ function. After the rabbits were euthanized, their kidneys and other organs (heart, liver, spleen, lungs, and intestines) were immersed in a 4% paraformaldehyde solution for fixation. Subsequently, 4 μm thick paraffin sections were prepared from the fixed organs for further analysis. Hematoxylin and eosin (H&E) staining was conducted *via* standard clinical laboratory techniques. The stained sections were then examined under a light microscope to assess the effects of the embolization treatment and identify any potential systemic toxicity.

2.12. Establishment of a rabbit orthotopic liver transplantation tumor model

The efficacy of MegaSphere as an embolic agent in TACE therapy was evaluated in a rabbit VX2 liver orthotopic transplantation tumor model. Fourteen healthy New Zealand white rabbits, with a weight of 2.5 to 3.0 kg, were carefully chosen for the experiment, regardless of sex. The modeling procedure involved anesthetizing the rabbits with 5% isoflurane for induction and 3.5% isoflurane for maintenance. First, VX2 cells were injected into the inner thigh muscles of two rabbits to induce tumor growth. Once the tumor in the thigh of the tumor-bearing rabbits reached a diameter of 2 cm, it was surgically removed. The vigorously growing tissue from the tumor parenchyma was collected, cut into $2 \times 2 \times 2$ mm^3 blocks, and stored in fresh medium at low temperature. Next, the tumor blocks were implanted. The rabbits were anesthetized and placed in the supine position on the operating table. The surgical area on the upper abdomen was shaved and disinfected in preparation for the procedure. A 4 cm longitudinal incision was made below the sternum along the midline of the abdomen to expose the left lobe of the liver. The prepared tumor blocks were then implanted into the left lobe of the liver. Finally, the abdomen was carefully sutured layer by layer, and the surgical area was disinfected. During the implantation of the tumor blocks, strict aseptic surgical techniques were used. After surgery, the rabbits were monitored in the animal laboratory until they recovered from anesthesia. Two weeks after the model surgery, a MRI scan of the upper abdomen was performed. The establishment of a successful liver cancer model was confirmed if the intrahepatic tumor had grown to a diameter of approximately 1.5 cm.

2.13. TACE treatment for liver cancer

TACE treatment for liver cancer was initiated after confirming the successful establishment of the liver orthotopic transplantation tumor model through MRI scanning. All surgeries were conducted by two experienced interventional radiologists in a dedicated sterile interventional surgery room. The experimental rabbits were randomly divided into four groups ($n = 3$) as follows: a blank control group, MegaSphere group, CalliSphere group, and DC Bead group. The rabbits were anesthetized with isoflurane (5% induction and 3.5% maintenance) before the procedure. Blood samples were collected from the marginal ear vein for routine blood tests, coagulation tests, blood biochemical analysis, and relevant inflammatory factor tests. The TACE procedure began with the exposure of the right femoral artery. A 4-F catheter sheath was then inserted into the femoral artery using a guide wire for guidance (Cook Company, USA). The 4-F catheter (Cook Company, USA) was carefully advanced into the abdominal aorta, and DSA (AXIOM-Artis, DSA system, Siemens, Germany) was performed. Iopromide, a contrast agent, was injected *via* a high-pressure injector with a single injection volume of 4 mL at a speed of 1.0 mL s^{-1}. The abdominal vascular distribution was examined to identify the hepatic tumor-feeding arteries. A 2.6-F microcatheter system (Progreat, Terumo, Japan) was subsequently introduced through the 4-F catheter. The microcatheter was carefully positioned within the hepatic tumor-feeding artery, followed by another angiography to verify the tumor-feeding artery and the precise location of the microcatheter. 300 mg of MegaSphere, CalliSphere or DC Bead were subsequently dispersed in 3 mL of PBS containing Dox (25 mg) to obtain MegaSphere-Dox, CalliSphere-Dox and DC Bead-Dox. Each rabbit received a slow injection of 1 mL of the appropriate microsphere suspension through the microcatheter. After the injection of the embolic agents, a slow flush of 2 mL of 0.9% saline was administered through the catheter. The animals in the blank control group received a 3 mL injection of saline through the microcatheter. The microcatheter and guide wire were subsequently carefully removed, and follow-up angiography was conducted *via* a 4-F catheter to assess the tumor blood supply. The femoral artery above the catheter sheath insertion site was permanently ligated with sutures. Finally, the surgical wound was meticulously sutured in layers and disinfected locally, and the TACE procedure was successfully completed.

2.14. *In vivo* antitumor activity monitoring with MRI

MRI was employed to monitor the therapeutic efficacy on liver tumors. Prior to TACE treatment and 7 days post-TACE treatment, T1- and T2-weighted images were obtained for all rabbits *via* a 9.4-T MR imaging scanner (GE Discovery MR750 Plus, USA). All the acquired images were analyzed by two radiologists with more than 10 years of clinical experience. The long and short diameters of each tumor, as well as the tumor volume (V), were evaluated *via* MRI. The tumor volume was calculated *via* the formula $V = 1/2ab^2$, where 'a' and 'b' represent the long and short diameters, respectively.

2.15. Hematological and pathological evaluation

Blood samples were collected from the marginal ear vein before surgery and on the 7th day post-surgery to conduct routine blood tests; assess coagulation function, cardiac function, hepatic

function, and renal function; and detect relevant inflammatory factors. In addition, the *in vivo* toxicity of the drug-loaded microspheres was further evaluated through histopathological examination. On the 7th day after the operation, all the animals in each group were euthanized, and the hearts, livers, spleens, lungs, kidneys, and pancreases of the experimental animals were collected. The tissues were fixed in a 10% formalin solution, embedded in paraffin, and sliced into sections with a thickness of approximately 4 μm. The sections from each group of tissues were stained with H&E for the evaluation of *in vivo* toxicity. Furthermore, the post-embolization efficacy was assessed through histopathological examination of the tumor and adjacent tissues. This evaluation included H&E staining and immunohistochemical examination. H&E staining was used to observe the appearance of the embolic microspheres, vascular occlusions, and extent of tumor tissue necrosis. Ki-67 immunostaining was utilized to evaluate tumor proliferation, whereas TUNEL staining was employed to assess apoptosis. CD31 staining and VEGF staining were used to assess the expression of angiogenesis-related factors within the tumor, whereas HIF-1α staining was utilized to detect tissue hypoxia. The immunohistochemical staining results were analyzed *via* ImageJ software. The pathological findings were assessed by two experienced pathologists with over 5 years of expertise, who conducted the evaluations in a blinded manner.

2.16. Statistical analysis

Statistical analysis was conducted *via* PRISM 8 software (GraphPad Software, San Diego, CA). The results are presented as the means ± SDs. For determination of statistical significance, either one-way ANOVA or unpaired two-tailed Student's *t* tests were performed *via* IBM SPSS 19.0 software.

3. Results and discussion

The MegaSphere microspheres were composed of polyvinyl alcohol and appeared blue (Fig. S1, ESI†). Optical microscope images revealed that both MegaSphere and drug-loaded MegaSphere-Dox exhibited spherical shapes with smooth surfaces, with an average particle size of 242.5 ± 50.9 μm (Fig. 1(A)). The fluorescence microscopy images revealed that the morphology of MegaSphere remained largely unchanged after loading with Dox (Fig. 1(B)). Confocal microscopy cross-sectional scanning images revealed uniform loading of Dox or Cy5.5 within MegaSphere (Fig. 1(C)), indicating a consistent and uniform structure of MegaSphere. The particle size, morphology, and surface of MegaSphere did not significantly change after drug loading. Scanning electron microscopy images revealed a smooth surface of the MegaSphere microspheres, without notable protrusions, angles, or depressions (Fig. S2A, ESI†). The interior of the microspheres exhibited a microporous structure (Fig. S2B, ESI†), which can increase the drug loading capacity. Moreover, the FTIR spectrum of the MegaSphere microspheres displayed a prominent vibration peak at 3417 cm^{-1}, indicating the abundance of hydroxyl groups within the microspheres (Fig. S2C, ESI†).

Optical microscopy demonstrated that the application of an external force caused the MegaSphere microspheres to deform, transforming into ellipsoidal or even flattened structures (Fig. 1(D)). Upon the removal of external pressure, the MegaSphere microspheres completely restored their original shape, indicating an excellent elastic deformation capability (Fig. 1(E)). The average Young's modulus of the MegaSphere microspheres, measured using nanoindentation experiments, is 9.77 ± 1.4 GPa. This demonstrates that the MegaSphere microspheres possess excellent deformation capability and elastic recovery. Furthermore, we conducted dynamic observations *via* optical microscopy, which revealed the smooth passage of MegaSphere microspheres through capillary glass tubes (Fig. 1(F)). The MegaSphere microspheres filled the narrower lumen of the capillary glass tube through elastic deformation, resulting in a tight and compact arrangement of the microspheres. Some microspheres exhibited compressed deformation, with minimal gaps observed between them (Fig. 1(F)). The *in vitro* embolization effect of the MegaSphere-Dox microspheres was subsequently evaluated *via* decellularized livers obtained from SD rats. After injecting the MegaSphere-Dox microspheres into the main portal vein of the decellularized liver, we observed successful filling of the vascular lumens within the portal system. The MegaSphere-Dox microspheres were densely packed within multiple levels of vascular branches, extending all the way to the terminal vasculature (Fig. 1(G)). The MegaSphere microspheres not only caused embolization within the main vessels but also exhibited deformation, allowing them to enter and embolize the lumens of distal vessels (Fig. 1(G)). These results suggest that our MegaSphere microspheres possess good elastic deformation capabilities, allowing them to adapt to various vascular levels. This ability to withstand increased external pressure enables graded and terminal vascular embolization, making them potentially suitable for achieving the desired therapeutic outcomes.

The drug-loading efficacy of the MegaSphere microspheres was compared to that of the clinically utilized CalliSphere microspheres (Fig. S3, ESI†). The MegaSphere microspheres achieved a drug loading capacity of 100 mg g^{-1} Dox within 30 min, which was 20% greater than that of the CalliSphere microspheres (Fig. 2(A)). A FBS solution (5% saline, pH 7.4) was used as the release medium to investigate the *in vitro* drug release behavior of the MegaSphere microspheres. The findings indicated that the release rate of Dox from MegaSphere-Dox was lower than that of the clinically employed CalliSphere-Dox (Fig. 2(B)). On the 7th day, the Dox release rate from MegaSphere-Dox was 23.5 ± 3.6%, whereas the release rate from CalliSphere-Dox was 40.2 ± 3.4%. The extended release profile has potential for sustained antitumor effects, offering good clinical application value.

A hemolysis test was performed using different concentrations of MegaSphere microspheres. The resulting supernatants from the MegaSphere samples at various concentrations appeared to be nearly transparent, indicating minimal hemolysis rates (Fig. 2(C)). The absorbance of hemoglobin at 540 nm was measured in each group to provide a quantitative assessment of the hemolytic effect caused by MegaSphere microspheres. The hemolysis rates corresponding to the MegaSphere

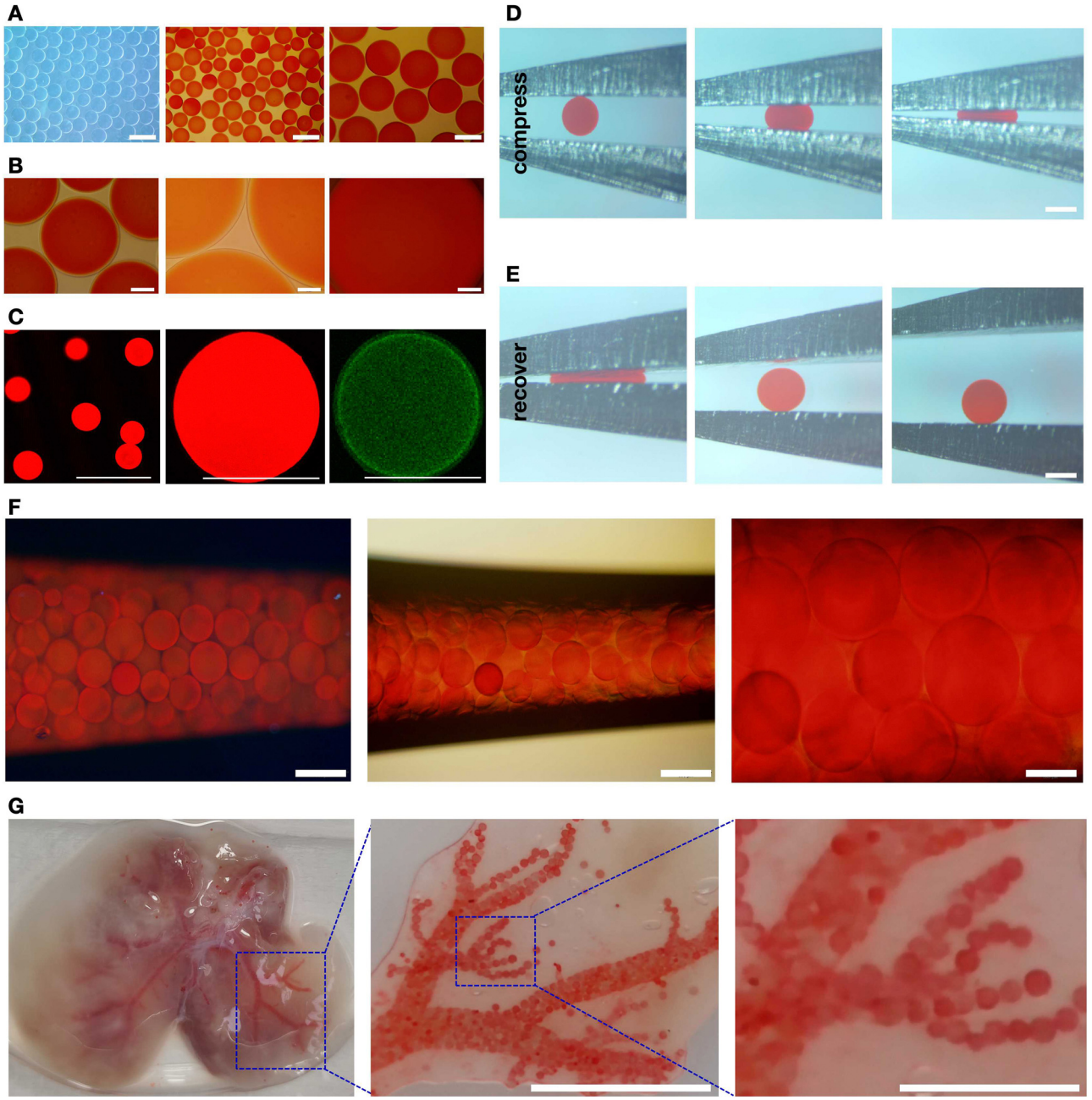

Fig. 1 (A) The left light blue image is an optical microscope image of MegaSphere microspheres. The middle and right images are optical microscope images of MegaSphere microspheres loaded with Dox. Scale bars from left to right: 500 μm, 500 μm, and 200 μm. (B) Optical microscope images depicting the contour and surface condition of the MegaSphere-Dox microspheres. Scale bars from left to right: 100 μm, 50 μm, and 50 μm. (C) The two images on the left are confocal microscope images of MegaSphere microspheres loaded with Dox. The image on the right is a confocal microscope image of MegaSphere microspheres loaded with Cy5.5. Scale bar from left to right: 500 μm, 100 μm, and 100 μm. (D) Optical microscopy images of the compression process of MegaSphere-Dox microspheres. Scale bar: 200 μm. (E) Optical microscopy images depicting the morphological recovery process of MegaSphere-Dox microspheres. Scale bar: 200 μm. (F) Optical microscopy images of MegaSphere-Dox microspheres embolized in a capillary glass tube. Scale bars from left to right: 500 μm, 500 μm, and 100 μm. (G) Optical microscopy image of MegaSphere-Dox microspheres injected into the portal vein of a decellularized liver. Scale bars from left to right: 2 cm and 1 cm.

concentrations of 1, 2, 4, 8, 10 and 15 mg mL^{-1} were measured to be 1.4%, 1.4%, 1.4%, 1.83%, 1.87%, and 2.6%, respectively. The negative control group had a hemolysis rate of 1.2%, whereas the positive control group had a significantly high rate of 98.43% (Fig. 2(D)). These findings indicate that MegaSphere microspheres exhibit excellent blood compatibility.

MegaSpheres at different concentrations were incubated with HepG2 cells for 24 and 48 h to evaluate their cytotoxicity (Fig. 2(E)). There was no significant difference in the viability of HepG2 cells incubated with MegaSphere compared with that of the negative control group after 24 and 48 h. The survival rates of HepG2 cells after incubation at a MegaSphere concentration

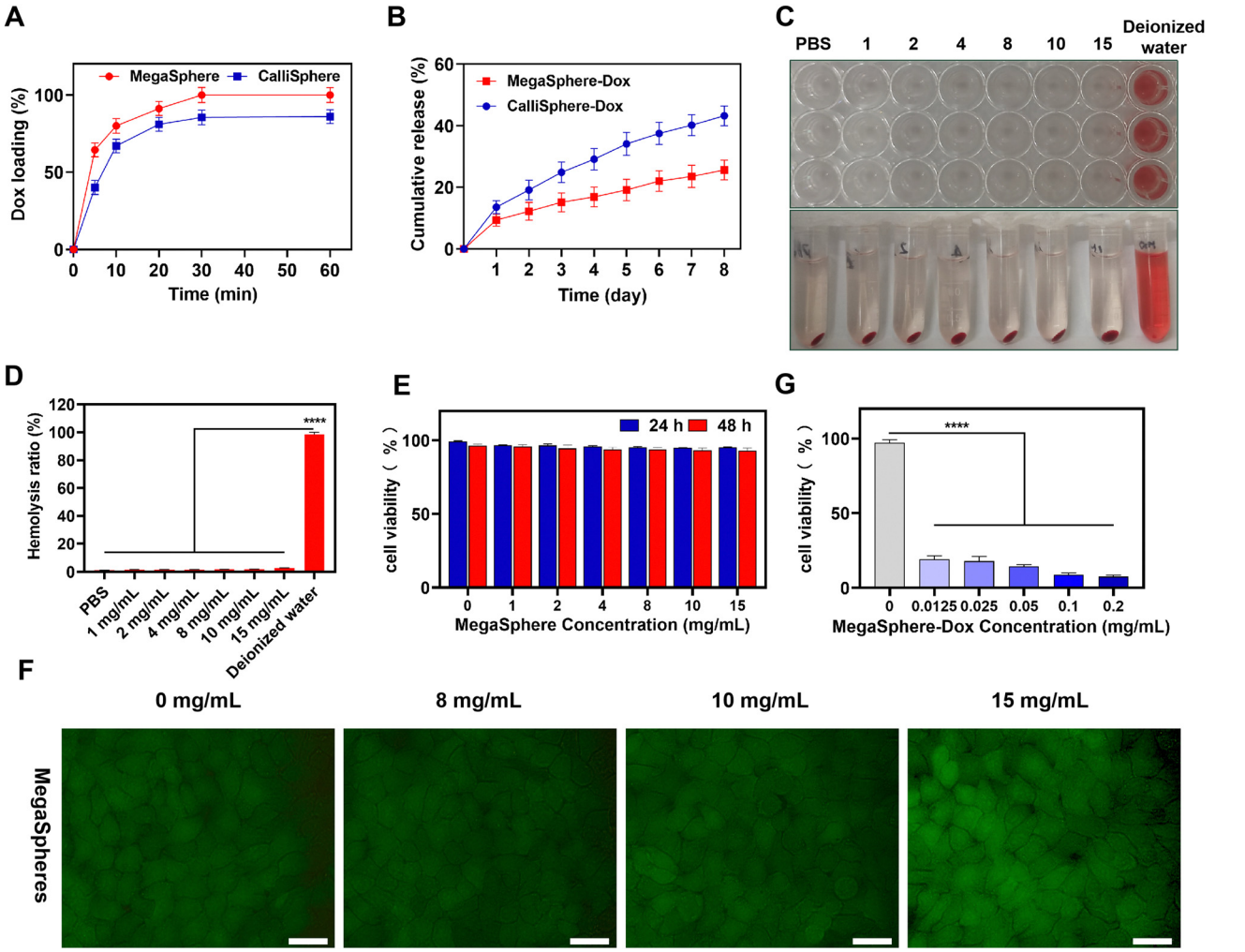

Fig. 2 (A) *In vitro* drug loading of MegaSphere and CalliSphere microspheres. (B) *In vitro* drug release of MegaSphere-Dox and CalliSphere-Dox microspheres. (C) *In vitro* hemocompatibility assessment of MegaSphere microspheres. (D) Absorbance values of the supernatant from red blood cell solutions incubated with MegaSphere microspheres (****$p < 0.0001$). (E) Cell viability of HepG2 cells co-incubated with MegaSphere microspheres for 24 and 48 h (n = 3, mean ± SD). (F) Live/dead cell staining results of HepG2 cells after 24 h of incubation with various concentrations of MegaSphere microspheres. Scale bar: 50 μm. (G) Cell viability of HepG2 cells co-incubated with MegaSphere-Dox microspheres for 24 h (n = 3, mean ± SD).

of 15 mg mL^{-1} for 24 and 48 h were 95.16% and 92.96%, respectively. Furthermore, live/dead cell staining of HepG2 cells revealed that both the negative control group and the MegaSphere group exhibited normal spindle-shaped growth after 48 h of incubation (Fig. 2(F)). The strong green fluorescence in the images indicates high viability of the HepG2 cells, which demonstrates that MegaSphere has excellent biocompatibility.

The cell viability was subsequently assessed by incubating HepG2 cells with different concentrations of MegaSphere-Dox in a 96-well plate for 24 h. After a 24 h incubation period with MegaSphere-Dox, the viability of HepG2 cells was significantly lower than that of the control group (Fig. 2(G)). At a MegaSphere-Dox concentration of 0.0125 mg mL^{-1}, the cell viability was notably low at 19.2%. The cell viability gradually decreased as the concentration of Megasphere-Dox increased. At a MegaSphere-Dox concentration of 0.2 mg mL^{-1}, the cell viability sharply decreased to 7.49%. These findings indicate that MegaSphere-Dox can effectively impede the growth of tumor cells, highlighting its potential in antitumor cell therapy.

A renal embolization experiment was carried out in rabbits to assess the *in vivo* embolization effectiveness of MegaSphere microspheres (Fig. 3(A)). For comparison, unilateral catheter-based renal artery embolization was conducted in each rabbit. The complete embolization procedure was monitored *via* DSA. Prior to embolization, all the groups presented normal renal artery morphology, robust renal parenchymal blood flow, and distinct kidney shapes and contours (Fig. 3(B)). DSA-guided embolization indicated that MegaSphere microspheres could be effectively delivered through the catheter, ensuring consistent distribution within the renal artery and its branches. Postembolization angiography revealed that the renal vasculature was nearly imperceptible and there was no contrast agent uptake in the renal parenchyma (Fig. 3(B)). This observation indicates that the MegaSphere microspheres achieved complete embolization, comparable to the clinically utilized CalliSphere and DC Bead microspheres, showing excellent *in vivo* vascular embolization efficacy.

On the 7th day after embolization, follow-up CT scans of both kidneys revealed a notably lower density in the embolized kidney than in the nonembolized contralateral kidney (Fig. 3(C)). Quantitative analysis revealed that the CT values of the embolized kidneys in all groups were substantially lower than those of the nonembolized kidneys, demonstrating significant differences (****$p < 0.0001$) (Fig. 3(C)). In the MegaSphere group, the CT values of the nonembolized and embolized kidneys were 64.33 ± 1.53 HU and 17.33 ± 1.53 HU, respectively; in the CalliSphere group, these values were 64.00 ± 2.65 HU and 17.66 ± 0.58 HU,

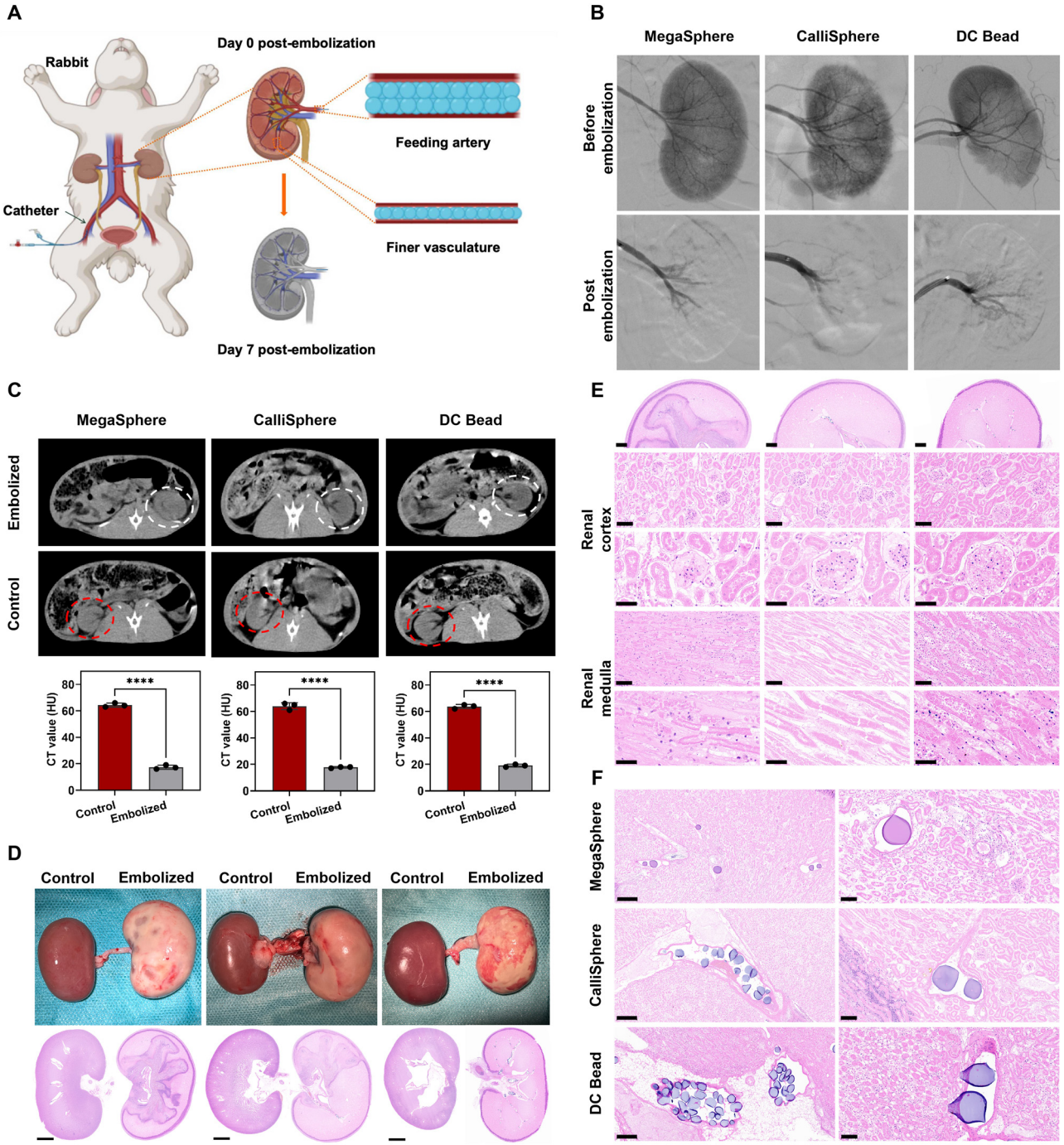

Fig. 3 (A) Schematic illustration of microsphere embolization in the rabbit kidney. (B) DSA images depicting the left kidneys of three rabbit groups before and after embolization. (C) CT scans of the kidneys taken 7 days after renal artery embolization. CT value analysis was conducted between the left kidney and the contralateral kidney following renal embolization (n = 3, mean ± SD, Student's t test, ****$p < 0.0001$). (D) Images of the kidneys taken 7 days after embolization, along with the corresponding H&E-stained histological sections along the kidney's longitudinal axis (n = 3). Scale bar: 5 cm. (E) Detailed pathological images of the renal cortex and medulla post-embolization. Scale bars from top to bottom: 2000 μm, 100 μm, 50 μm, 100 μm, and 50 μm. (F) Images showing embolic microspheres filling the blood vessels of the embolized kidney. Scale bars from left to right: 500 μm and 100 μm.

respectively; and in the DC Bead group, they were 63.66 ± 1.53 HU and 19.0 ± 1.0 HU respectively. These findings suggest that kidneys treated with the MegaSphere microspheres displayed ischemic infarction and edema post-embolization.

Moreover, examination of the gross kidney samples dissected on the 7th day after embolization in each group revealed that the embolized kidneys appeared white and exhibited a larger volume than the contralateral kidneys (Fig. 3(D)). These findings suggest that ischemic infarction results from the obstruction of oxygen and nutrient supplies during embolization. The swelling of the embolized kidneys is most likely attributed to inflammatory reactions, tissue edema, and necrosis that occur after embolization.[32] H&E staining of pathological tissue sections longitudinally cut along the embolized kidney revealed renal parenchyma necrosis on the embolized side with a blurred corticomedullary boundary (Fig. 3(D)). Comparative evaluation of the embolization outcomes of the MegaSphere, CalliSphere, and DC Bead groups revealed that across all the embolized groups, a substantial portion of the renal cortex and medulla displayed necrosis, consistent with features typical of ischemic infarction. Detailed microscopic examination of H&E-stained images of the embolized kidneys revealed that in the MegaSphere, CalliSphere, and DC Bead groups, the typical structure of the glomeruli and renal tubules was no longer discernible. These results suggest that the MegaSphere microspheres effectively embolize blood vessels similar to the CalliSphere and DC Bead microspheres, resulting in tissue necrosis post-embolization (Fig. 3(E)). Furthermore, detailed microscopy revealed that the MegaSphere microspheres were predominantly located within the deep blood vessels of the renal parenchyma, with deformed microspheres observed in the blood vessels of the deep renal cortex and medulla (Fig. 3(F)). In contrast, the CalliSphere and DC Bead microspheres tended to accumulate in the main renal artery and larger branch arteries, with minimal presence in smaller vessels (Fig. 3(F)). The results demonstrate that MegaSphere microspheres have the greatest potential to achieve better embolization.[33]

Additionally, we assessed the condition of other organs 7 days post-embolization through CT images (Fig. 4(A)). No notable abnormalities were detected upon analyzing the CT images and CT values of the brains, hearts, livers, and lungs in the MegaSphere, CalliSphere, and DC Bead groups. The CT values of these organs fell within the normal range and did not significantly differ from those of the control group (Fig. 4(B)). These findings indicate the absence of off-target embolization in the brain, heart, liver, and lungs. Moreover, we examined the pathological outcomes of key organs (contralateral kidneys, hearts, livers, lungs, and intestines) post-embolization in the MegaSphere, CalliSphere, and DC Bead groups. The results revealed no notable tissue damage, inflammation, necrosis, or fibrosis in these organs (Fig. 4(C)), indicating that MegaSphere does not induce ectopic embolization.

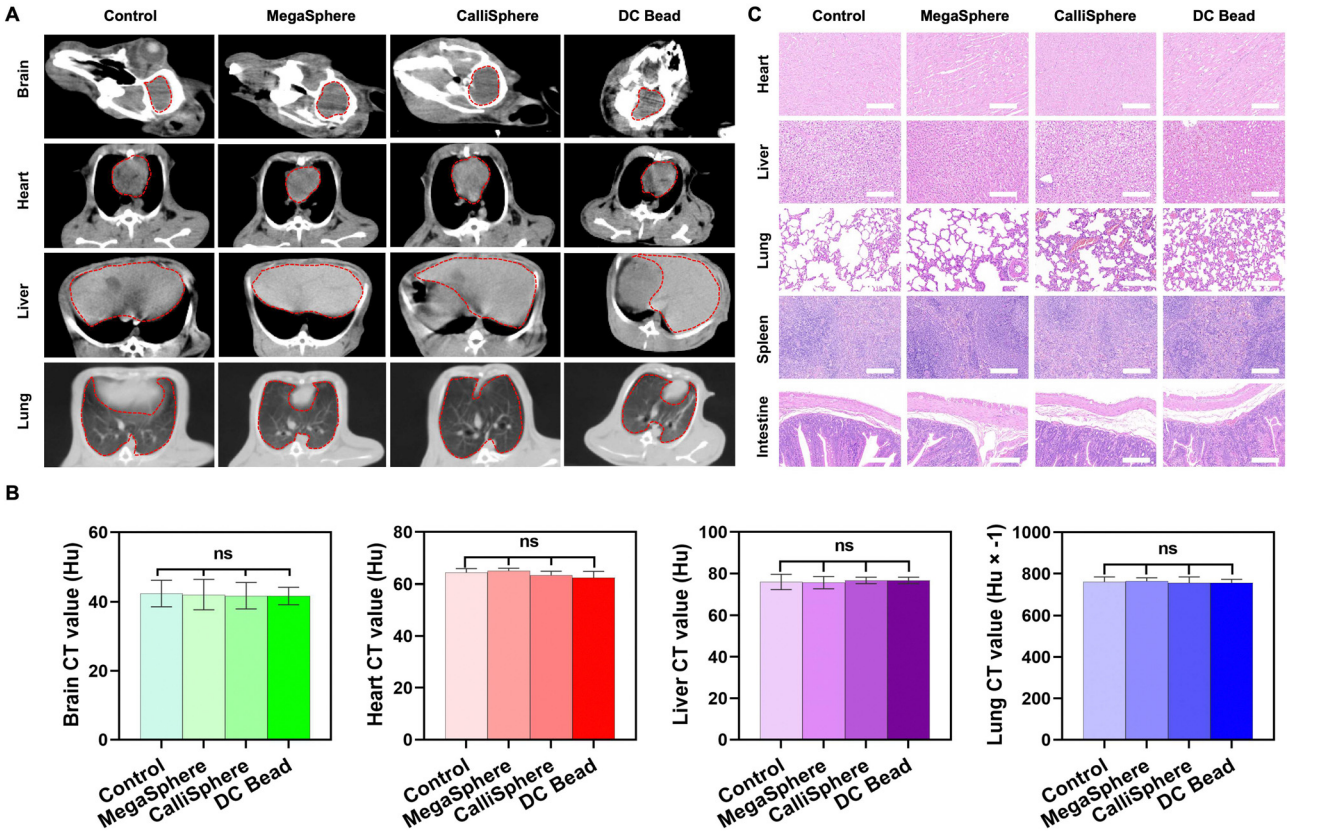

Fig. 4 (A) CT scan images of rabbits in the control group, MegaSphere group, CalliSphere group, and DC Bead group. (B) Statistical analysis results of CT values for each organ in each group (n = 3, mean ± SD). (C) Post-embolization pathological histological examination of the heart, liver, lung, spleen, and small intestine of rabbits in each group after treatment. Scale bar: 200 μm.

Blood samples were taken from each rabbit group prior to embolization and on the 7th day post-embolization to investigate potential systemic side effects following kidney embolization with MegaSphere. Standard blood tests, along with assessments of heart, liver, and kidney functions, as well as blood coagulation, were performed. The results indicated that all of the values were within normal ranges. Additionally, tests for inflammation-related markers (interleukin-1β, interleukin-6, transforming growth factor-α, and procalcitonin) were carried out. Hematology tests revealed that all blood parameters were within normal limits (Fig. S4, ESI†). After embolization, the creatinine levels in the MegaSphere, CalliSphere and DC Bead groups remained within the normal range, albeit higher than the pre-embolization levels. Furthermore, there were no notable effects on liver function, coagulation function, cardiac function, or kidney function, suggesting that MegaSphere microspheres do not demonstrate notable hematotoxicity or *in vivo* toxicity. Moreover, the levels of proinflammatory factors (IL-1β, IL-6, TGF-α, and PCT) in the blood of rabbits in all the groups remained within normal ranges, suggesting the absence of a notable systemic inflammatory response after embolization. In summary, the hematological test results indicate that MegaSphere microspheres do not elicit substantial systemic toxicity or inflammatory reactions, meeting the established *in vivo* safety criteria for embolic agents.[34]

The rabbits were then randomly grouped for TACE treatment. After one week of follow-up, MRI was conducted to evaluate the effectiveness of the treatment, and embolized tumors along with visceral organs were dissected for pathological examination (Fig. 5(A)). Within each experimental group, the rabbits underwent TACE treatment *via* a microcatheter inserted into the hepatic artery through the femoral artery pathway, guided by DSA.[35] MegaSphere-Dox, CalliSphere-Dox, and DC Bead-Dox drug-loaded microspheres were administered into the liver tumors *via* a microcatheter. Pathological examination of the dissected tissues confirmed that the liver tumors were successfully embolized by the microspheres. Tissue necrosis was evident within the tumor mass upon dissection of the MegaSphere-Dox-embolized tumors (Fig. 5(B)). Initially, DSA images were used to examine the liver tumors in each rabbit group. Angiographic images revealed that the liver tumors were well-vascularized, with evident feeding arteries supplying them. DSA images revealed the disappearance of intrahepatic tumors in every group. The analysis revealed a clear hepatic artery embolization effect in each microsphere treatment group compared with the blank control group, resulting in complete cessation of the tumor blood supply (Fig. 5(C)). MRI assessments on the 7th day post-treatment revealed notable reductions in the size of liver tumors in the MegaSphere-Dox, CalliSphere-Dox, and DC Bead-Dox groups compared with their pretreatment sizes and those in the control group (Fig. 5(D)). MR images revealed that the average tumor volume in the control group increased 3.5-fold one week after treatment (Fig. 6(A)). Conversely, the MegaSphere-Dox, CalliSphere-Dox, and DC Bead-Dox groups presented substantially decreased tumor volumes compared with the blank control group. After one week of treatment, the average tumor volumes in the MegaSphere-Dox, CalliSphere-Dox, and DC Bead-Dox groups decreased by 46.37%, 32.11%, and 27.61%, respectively, compared with the pretreatment volumes. The short-term tumor volume reduction following embolization treatment is primarily attributed to tumor tissue necrosis, edema, and inflammatory infiltration in the immediate postembolization period.[36] Hence, the outcomes of the MegaSphere-Dox, CalliSphere-Dox, and DC Bead-Dox groups demonstrate effective suppression of tumor growth. Furthermore, H&E staining of tumor tissues from the MegaSphere-Dox group revealed that the microspheres filled the vascular lumen within the tumor tissue, alongside extensive areas of necrosis (Fig. 5(E)). The above findings indicate that MegaSphere-Dox effectively regulates tumor advancement in TACE antitumor therapy, demonstrating slightly better performance compared to CalliSphere-Dox and DC Bead-Dox. Additionally, it has been observed that the MegaSphere microspheres undergo a certain degree of deformation within the vascular lumen. The deformability makes the MegaSphere adapt to the embolization of terminal blood vessels within tumors.[37]

Additionally, for analysis of the systemic side effects of MegaSphere-Dox in TACE therapy for liver cancer, blood samples were collected from each rabbit group before embolization and on the 7th day after embolization for routine blood tests, coagulation function assessments, blood biochemical analyses and inflammatory factor evaluations (Fig. S5, ESI†). The alanine transaminase (ALT) and aspartate transaminase (AST) levels remained within normal limits. Other hematological test parameters exhibited no notable differences from pretreatment levels and fell within the normal range. These findings suggest that MegaSphere-Dox has minimal effects on standard blood parameters, liver functions, coagulation functions, cardiac functions, and kidney functions without inducing notable hematological toxicity. The inflammatory factor test results revealed that the levels of inflammatory markers in the blood of rabbits across all the groups remained within normal limits, suggesting that MegaSphere-Dox did not trigger notable systemic inflammatory reactions as a chemoembolization agent. MegaSphere-Dox demonstrated comparable *in vivo* safety to the other two commonly used clinical embolization microspheres. Hence, MegaSphere-Dox meets the criteria for *in vivo* safety and effective antitumor treatment in clinical TACE.

For further evaluation of the *in vivo* biosafety of MegaSphere-Dox, H&E staining analysis was conducted on the hearts, lungs, spleens, kidneys, and pancreases of the rabbits treated with MegaSphere-Dox, CalliSphere-Dox, and DC Bead-Dox (Fig. 6(B)). No significant differences were detected at the pathological level compared with those in the control group. The nuclei and cellular structures of the organs treated with MegaSphere-Dox appeared normal. These findings reinforce the good *in vivo* biosafety profile of MegaSphere-Dox, as this treatment did not induce notable systemic toxicity. These findings underscore that MegaSphere-Dox possesses the necessary *in vivo* safety credentials for use in TACE antitumor therapy.

Seven days post-TACE treatment, all rabbits were euthanized, and tumor tissues were harvested *via* pathological staining procedures. H&E staining specifically aimed to examine tumor tissue necrosis following treatment. Extensive areas of

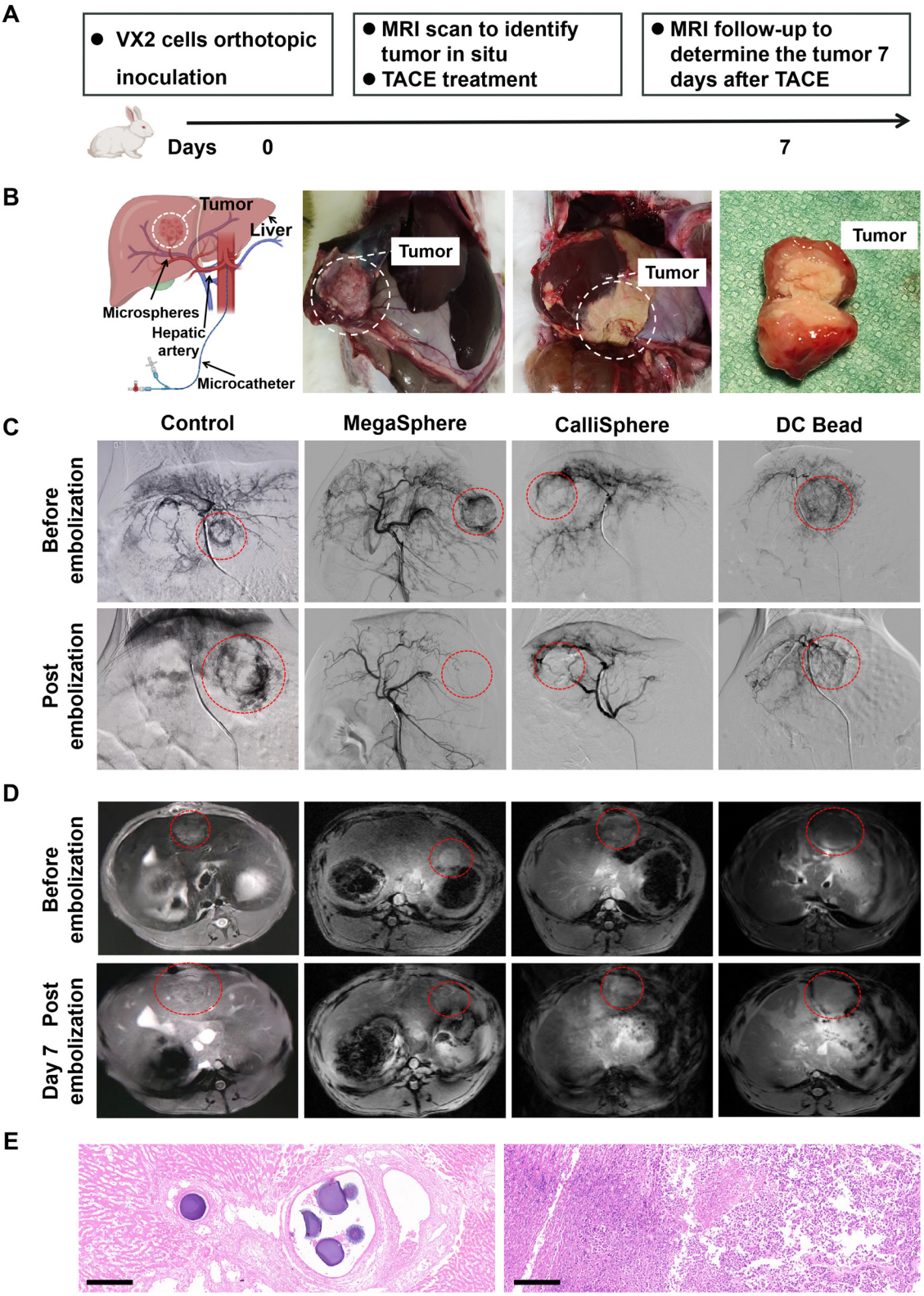

Fig. 5 (A) The flowchart of *in vivo* study of the TACE treatment process. (B) Schematic diagram of transcatheter hepatic arteriography and anatomical representation of liver tumor post-embolization. (C) DSA images of depicting each group before and after embolization. (D) MR images of showing each group before and 7 days after embolization. (E) H&E staining images of tumor tissue after 7 days of MegaSphere-Dox embolization. Scale bar: 200 μm.

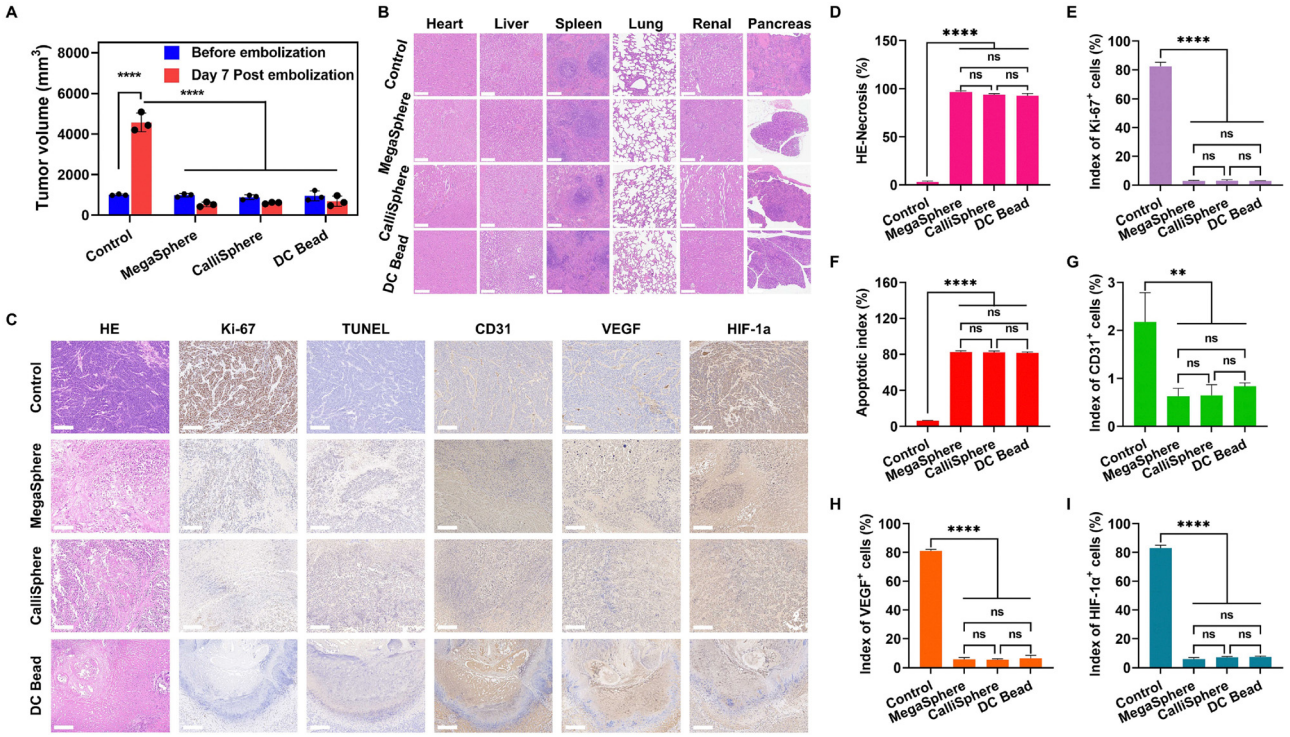

Fig. 6 (A) Comparative assessment of intrahepatic tumor diameter measured by MRI in each group (control: the control group, MegaSphere: MegaSphere-Dox group, CalliSphere: CalliSphere-Dox group, and DC Bead: DC Bead-Dox group) pre-TACE treatment and on the 7th day after post-treatment (****$P < 0.0001$). (B) H&E-stained tissue sections of the hearts, livers, spleens, lungs, kidneys, and pancreas of rabbits on the 7th day post-operation in each group are provided as representatives. Scale bar: 200 μm. (C) Illustrative images of H&E-staining, Ki-67, TUNEL, CD31, VEGF, and HIF-1α immunohistochemical (IHC) staining on tumor tissues in each group. Scale bar: 200 μm. (D)–(I) Quantitative analysis of H&E and immunohistochemical markers Ki-67, TUNEL, CD31, VEGF, and HIF-1α (day 7) in tumor tissues from different treatment groups ($n = 3$, mean ± SD, *$P < 0.05$).

necrosis were noted in the tumor tissue of the MegaSphere-Dox group (Fig. 6(C)). Similarly, patchy necrotic areas were identified in the tumor tissues of the CalliSphere-Dox and DC Bead-Dox groups (Fig. 6(D)). Conversely, the tumor regions in the blank control group presented densely packed nuclei. MegaSphere-Dox, CalliSphere-Dox, and DC Bead-Dox successfully induced liver tumor embolization and triggered tumor cell necrosis following hepatic artery injection, demonstrating their therapeutic efficacy.

Moreover, the immunohistochemical findings of tumor tissues in each group after TACE treatment were further examined. Ki-67 staining was utilized to assess tumor cell proliferation. The findings revealed that the percentages of Ki-67-positive cells in the control group, MegaSphere-Dox group, CalliSphere-Dox group, and DC Bead-Dox group were 82.44 ± 2.88%, 2.85 ± 0.42%, 2.99 ± 0.63%, and 2.88 ± 0.18%, respectively (Fig. 6(E)). The percentages of Ki-67-positive cells in the MegaSphere-Dox, CalliSphere-Dox, and DC Bead-Dox groups were notably lower than those in the control group. There was no significant difference among the MegaSphere-Dox, CalliSphere-Dox, and DC Bead-Dox groups, suggesting that MegaSphere-Dox has equally effective inhibitory effects on tumor cell proliferation as CalliSphere-Dox and DC Bead-Dox.

Concurrently, the apoptotic cell index was assessed through TUNEL staining, revealing values of 6.18 ± 0.53%, 82.34 ± 1.65%, 82.07 ± 1.58%, and 81.57 ± 1.09% for the control group, MegaSphere-Dox group, CalliSphere-Dox group, and DC Bead-Dox group, respectively (Fig. 6(F)). The TUNEL staining results demonstrated that the MegaSphere-Dox, CalliSphere-Dox, and DC Bead-Dox groups all presented elevated apoptosis rates in liver cancer after TACE treatment. The Ki-67 and TUNEL immunohistochemistry findings were consistent, illustrating the robust antitumor effects in the MegaSphere-Dox, CalliSphere-Dox, and DC Bead-Dox groups. The Ki-67 and TUNEL findings additionally suggest that MegaSphere-Dox has good antitumor efficacy comparable to that of the clinically employed CalliSphere-Dox and DC Bead-Dox.

Immunohistochemical staining additionally validated the impact of drug-loaded microspheres on the expression levels of CD31, VEGF, and HIF-1α in tumor tissues from the MegaSphere-Dox, CalliSphere-Dox, and DC Bead-Dox groups (Fig. 6(G)–(I)). The results show that MegaSphere-Dox reduces the expression levels of CD31, VEGF, and HIF-1α, which is most likely ascribed to the fact that substantial necrosis of tumor cells occurs after TACE treatment. These results further demonstrate that the MegaSphere-Dox enhances the effectiveness of transarterial chemotherapy embolization.

4. Conclusions

In summary, our research focused on MegaSphere, a unique type of embolic microsphere. These microspheres possess good elasticity, enabling them to conform to different shapes when

influenced by external forces, thereby assisting in the embolization of blood vessels of varying sizes. Furthermore, MegaSphere microspheres show exceptional drug loading and release capabilities, indicating good potential for continuous antitumor treatment. Our findings also affirm the favorable hemocompatibility and cytocompatibility of MegaSphere. Additionally, MegaSphere demonstrates adaptability to diverse blood vessel sizes in laboratory-based embolization models, reaching the distal parts of embolized vessels in rabbit kidney experiments, indicating superior distal vascular embolization compared with that of current clinical microspheres.

The experiments further confirmed the good *in vivo* safety of the drug-loaded MegaSphere-Dox microspheres. Moreover, the MegaSphere-Dox microspheres can effectively block the arterial blood supply to liver tumors while releasing Dox for localized therapy. In the arterial chemoembolization treatment of the rabbit liver VX2 transplant tumor model, MegaSphere-Dox exhibited excellent antitumor performance. Compared with the blank control, MegaSphere-Dox effectively inhibited the progression of intrahepatic tumors in the short term. Furthermore, in a comparison of MegaSphere-Dox to the clinically used CalliSphere-Dox and DC Bead-Dox drug-loaded microspheres, no significant difference was found in terms of antitumor treatment efficacy, indicating that MegaSphere-Dox had excellent therapeutic effects. These findings demonstrate the potential of the MegaSphere as a novel highly elastic and drug-loaded microsphere in arterial embolization therapy for vascular-related and tumorous diseases. Finally, the main limitation of this study lies in the gap between assessing efficacy in animal models and real-world treatments, indicating the need for further clinical trials to validate the efficacy of MegaSphere in arterial catheter embolization therapy applications.

Author contributions

Li Liu: conceptualization, data curation, methodology, writing – original draft, project administration, validation, resources, software, formal analysis, and visualization. Xiangxian Xu: data curation and methodology. Xiaoli Zhu: supervision. Meng Dang: methodology. Yunming Zhang: methodology. Donghong Shi: methodology. Shenzhe Liu: methodology. Zhiwei Zhang: methodology. Jing Pan: methodology. Jing Zhong: methodology. Lin Ou-yang: supervision and resources. Zhaogang Teng: conceptualization, supervision, resources, validation, writing – review & editing, and project administration. Longjiang Zhang: supervision, resources, and writing – review & editing.

Data availability

Data will be made available on request.

Conflicts of interest

The authors declare that they have no known competing financial interests or personal relationships that could have appeared to influence the work reported in this paper.

Acknowledgements

We greatly appreciate the financial support from the National Natural Science Foundation of China (82302321, 81971675 and 22275099) and the Youth Fund of Jinling Hospital, China (YYQN2021069).

References

1 R. J. Lewandowski, J. F. Geschwind, E. Liapi and R. Salem, Transcatheter intraarterial therapies: rationale and overview, *Radiology*, 2011, **259**, 641–657.
2 J. Hu, H. Albadawi, B. W. Chong, A. R. Deipolyi, R. A. Sheth, A. Khademhosseini and R. Oklu, Advances in biomaterials and technologies for vascular embolization, *Adv. Mater.*, 2019, **31**, e1901071.
3 E. Liapi and J. F. Geschwind, Transcatheter and ablative therapeutic approaches for solid malignancies, *J. Clin. Oncol.*, 2007, **25**, 978–986.
4 A. Poursaid, M. M. Jensen, E. Huo and H. Ghandehari, Polymeric materials for embolic and chemoembolic applications, *J. Controlled Release*, 2016, **240**, 414–433.
5 Y. Ma, Z. Li, Y. Luo, Y. Chen, L. Ma, X. Liu, J. Xiao, M. Huang, Y. Li, H. Jiang, M. Wang, X. Wang, J. Li, J. Kong, P. Shi, H. Yu, X. Jiang and Q. Guo, Biodegradable microembolics with nanografted polyanions enable high-efficiency drug loading and sustained deep-tumor drug penetration for locoregional chemoembolization treatment, *ACS Nano*, 2024, **18**, 18211–18229.
6 L. Liu, X. Liang, X. Xu, X. Zhang, J. Wen, K. Chen, X. Su, Z. Teng, G. Lu and J. Xu, Magnetic mesoporous embolic microspheres in transcatheter arterial chemoembolization for liver cancer, *Acta Biomater.*, 2021, **130**, 374–384.
7 X. Liu, T. Hu, Y. Jia, S. Yang, Y. Yang, Z. Cui, T. Wang, R. Liang, C. Tan and Y. Wang, A MgAl-LDH-CuS nanosheet-based thermo-responsive composite hydrogel with nir-responsive angiogenesis inhibitor releasing capability for multimode starvation therapy, *J. Nanobiotechnol.*, 2024, **22**, 127.
8 R. C. Gaba, R. Emmadi, A. Parvinian and L. C. Casadaban, Correlation of doxorubicin delivery and tumor necrosis after drug-eluting bead transarterial chemoembolization of rabbit VX2 liver tumors, *Radiology*, 2016, **280**, 752–761.
9 S. Hong, W. S. Choi, B. Purushothaman, J. Koh, H. C. Kim, J. W. Chung, J. M. Song and J. W. Choi, Drug delivery in transarterial chemoembolization of hepatocellular carcinoma: *ex vivo* evaluation using transparent tissue imaging, *Acta Biomater.*, 2022, **154**, 523–535.
10 D. Wang and W. Rao, Bench-to-bedside development of multifunctional flexible embolic agents, *Theranostics*, 2023, **13**, 2114–2139.
11 A. Zhang, Z. Xiao, Q. Liu, P. Li, F. Xu, J. Liu, H. Tao, L. Feng, S. Song, Z. Liu and G. Huang, $CaCO_3$-encapuslated microspheres for enhanced transhepatic arterial embolization treatment of hepatocellular carcinoma, *Adv. Healthcare Mater.*, 2021, **10**, e2100748.
12 L. Du, Y. Huang, Q. Zhang, Y. Zhou, J. Huang, L. Yan, Z. Yu, A. Qin, H. Yang, M. Chen, L. Liang, B. Bian, X. Li and J. Fu,

Synthesis and assessment of drug-eluting microspheres for transcatheter arterial chemoembolization, *Acta Biomater.*, 2019, **88**, 370–382.

13 F. Gao, M. Rafiq, H. Cong, B. Yu and Y. Shen, Current research status and development prospects of embolic microspheres containing biological macromolecules and others, *Int. J. Biol. Macromol.*, 2024, **267**, 131494.

14 G. Chen, R. Wei, X. Huang, F. Wang and Z. Chen, Synthesis and assessment of sodium alginate-modified silk fibroin microspheres as potential hepatic arterial embolization agent, *Int. J. Biol. Macromol.*, 2020, **155**, 1450–1459.

15 H. Dong, D. Yang, Y. Hu and X. Song, Recent advances in smart nanoplatforms for tumor non-interventional embolization therapy, *J. Nanobiotechnol.*, 2022, **20**, 337.

16 X. Li, X. Ji, K. Chen, M. W. Ullah, B. Li, J. Cao, L. Xiao, J. Xiao and G. Yang, Immobilized thrombin on X-ray radiopaque polyvinyl alcohol/chitosan embolic microspheres for precise localization and topical blood coagulation, *Bioact. Mater.*, 2021, **6**, 2105–2119.

17 J. Li, J. Xu, Y. Wang, Y. Chen, Y. Ding, W. Gao, Y. Tan, N. Ge, Y. Chen, S. Ge, Q. Yang, B. He and X. Ye, Fusible and radiopaque microspheres for embolization, *Adv. Mater.*, 2024, **9**, e2405224.

18 H. Choi, B. Choi, B. Yu, W. Li, M. M. Matsumoto, K. R. Harris, R. J. Lewandowski, A. C. Larson, S. K. Mouli and D. H. Kim, On-demand degradable embolic microspheres for immediate restoration of blood flow during image-guided embolization procedures, *Biomaterials*, 2021, **265**, 120408.

19 N. Yang, X. Sun, Y. Zhou, X. Yang, J. You, Z. Yu, J. Ge, F. Gong, Z. Xiao, Y. Jin, Z. Liu and L. Cheng, Liquid metal microspheres with an eddy-thermal effect for magnetic hyperthermia-enhanced cancer embolization-immunotherapy, *Sci. Bull.*, 2023, **68**, 1772–1783.

20 C. Wei, C. Wu, X. Jin, P. Yin, X. Yu, C. Wang and W. Zhang, CT/MR detectable magnetic microspheres for self-regulating temperature hyperthermia and transcatheter arterial chemoembolization, *Acta Biomater.*, 2022, **153**, 453–464.

21 K. Wu, S. Ma, X. Xu, Y. Liu, C. Tian, C. Zhang, J. Shan, Z. Li, K. Ren, J. Ren, X. Han and Y. Zhao, Celecoxib and cisplatin dual-loaded microspheres synergistically enhance transarterial chemoembolization effect of hepatocellular carcinoma, *Mater. Today Bio*, 2023, **24**, 100927.

22 Y. Tang, J. Zhang, D. He, W. Miao, W. Liu, Y. Li, G. Lu, F. Wu and S. Wang, GANDA: A deep generative adversarial network conditionally generates intratumoral nanoparticles distribution pixels-to-pixels, *J. Controlled Release*, 2021, **336**, 336–343.

23 L. Liu, X. Xu, X. Liang, X. Zhang, J. Wen, K. Chen, X. Su, Y. Ma, Z. Teng, G. Lu and J. Xu, Periodic mesoporous organosilica-coated magnetite nanoparticles combined with lipiodol for transcatheter arterial chemoembolization to inhibit the progression of liver cancer, *J. Colloid Interface Sci.*, 2021, **591**, 211–220.

24 L. Shi, D. Li, Q. Tong, G. Jia, X. Li, L. Zhang, Q. Han, R. Li, C. Zuo, W. Zhang and X. Li, Silk fibroin-based embolic agent for transhepatic artery embolization with multiple therapeutic potentials, *J. Nanobiotechnol.*, 2023, **21**, 278.

25 J. Hu, H. Albadawi, Z. Zhang, M. A. Salomao, S. Gunduz, S. Rehman, L. D'Amone, J. L. Mayer, F. Omenetto and R. Oklu, Silk embolic material for catheter-directed endovascular drug delivery, *Adv. Mater.*, 2022, **34**, e2106865.

26 J. Han, A. S. Guenier, S. Salmieri and M. Lacroix, Alginate and chitosan functionalization for micronutrient encapsulation, *J. Agric. Food Chem.*, 2008, **56**, 2528–2535.

27 K. Hidaka, M. Nakamura, K. Osuga, H. Miyazaki and S. Wada, Elastic characteristics of microspherical embolic agents used for vascular interventional radiology, *J. Mech. Behav. Biomed. Mater.*, 2010, **3**, 497–503.

28 K. Fuchs, R. Duran, A. Denys, P. E. Bize, G. Borchard and O. Jordan, Drug-eluting embolic microspheres for local drug delivery - state of the art, *J. Controlled Release*, 2017, **262**, 127–138.

29 A. Pérez-López, C. Martín-Sabroso, L. Gómez-Lázaro, A. I. Torres-Suárez and J. Aparicio-Blanco, Embolization therapy with microspheres for the treatment of liver cancer: State-of-the-art of clinical translation, *Acta Biomater.*, 2022, **149**, 1–15.

30 X. Liu, X. Wang, Y. Luo, M. Wang, Z. Chen, X. Han, S. Zhou, J. Wang, J. Kong, H. Yu, X. Wang, X. Tang and Q. Guo, A 3D tumor-mimicking in vitro drug release model of locoregional chemoembolization using deep learning-based quantitative analyses, *Adv. Sci.*, 2023, **10**, e2206195.

31 Y. Gao, Z. Li, Y. Hong, T. Li, X. Hu, L. Sun, Z. Chen, Z. Chen, Z. Luo, X. Wang, J. Kong, G. Li, H. L. Wang, H. L. Leo, H. Yu, L. Xi and Q. Guo, Decellularized liver as a translucent *ex vivo* model for vascular embolization evaluation, *Biomaterials*, 2020, **240**, 119855.

32 A. Kónya, C. S. Van Pelt and K. C. Wright, Ethiodized oil-ethanol capillary embolization in rabbit kidneys: temporal histopathologic findings, *Radiology*, 2004, **232**, 147–153.

33 Q. Bi, Y. Li, R. Luo, H. Chen, Y. Lv, Z. Liu, Q. Liang, L. Chen, B. Xu and Q. Tang, Pi-inducedin-situaggregation of sevelamer nanoparticles for vascular embolization, *Nanotechnology*, 2022, **33**, 355101.

34 B. Wan, Q. Bao and D. Burgess, Long-acting PLGA microspheres: advances in excipient and product analysis toward improved product understanding, *Adv. Drug Delivery Rev.*, 2023, **198**, 114857.

35 K. L. Liu, Z. C. Jin, X. L. Hu, D. Yan, Y. Zhang, H. D. Zhu, G. J. Teng and F. Xiong, A biodegradable multifunctional porous microsphere composed of carrageenan for promoting imageable trans-arterial chemoembolization, *Int. J. Biol. Macromol.*, 2020, **142**, 866–878.

36 R. Duran, J. Namur, F. Pascale, P. Czuczman, Z. Bascal, H. Kilpatrick, R. Whomsley, S. Ryan, A. L. Lewis and A. Denys, Vandetanib-eluting radiopaque beads: pharmacokinetics, safety, and efficacy in a rabbit model of liver cancer, *Radiology*, 2019, **293**, 695–703.

37 H. Chen, C. Xie, Y. Li, Z. Deng, Y. Lv, Q. Bi, J. Tang, R. Luo and Q. Tang, Evaluation of the safety and efficacy of transarterial sevelamer embolization in a rabbit liver cancer model: A challenge on the size rule for vascular occlusion, *Front. Bioeng. Biotechnol.*, 2022, **10**, 1058042.